Solvothermal Synthesis and Luminescent Properties of Two Organically Templated Chain-Structure Fluorides, $[C_4H_{14}N_2][MF_5]$ (M = In, Sc)

Anil C. A. Jayasundera,[†] Adrian A. Finch,[‡] Philip Wormald,[†] and Philip Lightfoot*,[†]

EaStChem, School of Chemistry, University of St. Andrews, St. Andrews, Fife KY16 9ST, United Kingdom, and School of Geography and Geosciences, University of St. Andrews, St. Andrews, Fife KY16 9AL, United Kingdom

Received July 28, 2008. Revised Manuscript Received September 22, 2008

The solvothermal syntheses and crystal structures of organically templated indium fluoride, $[C_4H_{14}N_2][InF_5]$ **1**, and its scandium analogue, $[C_4H_{14}N_2][ScF_5]$ **2**, are reported. Compound **1** represents the first indium fluoride with extended inorganic connectivity prepared using an organic amine, 1,4-diaminobutane (DAB), as a structure-directing agent. **1** is orthorhombic, space group *Ibam*, with cell parameters $a = 9.324(2)$ Å, $b = 11.391(2)$ Å, $c = 8.401(2)$, and $Z = 4$ (for isostructural **2**: $a = 9.353(3)$ Å, $b = 11.433$ (1) Å, $c = 8.226$ (4) Å). The structure of **1** consists of infinite *trans* vertex sharing $(InF_5)_\infty$ chains running parallel to the *c*-axis, which are linked via H-bonded organic moieties. The photoluminescence properties of the doped compounds, of nominal composition $[C_4H_{14}N_2][In_{1-x}Ln_xF_5]$ (Ln=Tb and/or Eu), have been explored. For $x = 0.05$ Eu^{3+}, **1** exhibits a dominant orange emission at 592.5 nm from the $^5D_0 \rightarrow {}^7F_1$ magnetic dipole transition within Eu^{3+}. For $x = 0.08$ Tb^{3+}, **1** shows strong down-conversion fluorescence corresponding to $^5D_4 \rightarrow {}^7F_5$ (green at 543.5 nm). In addition, a Tb^{3+}/Eu^{3+} co-doped sample exhibits a combination of green (Tb^{3+}) and orange (Eu^{3+}) luminescence, with Tb^{3+} enhancing the emission of Eu^{3+} in this host. The dependence of luminescence intensity on dopant concentration for **1** has been analyzed. The scandium and fluorine local environments in **2** have been characterized by ^{19}F and ^{45}Sc solid-state magic-angle spinning (MAS) NMR, which confirms a single scandium site together with discrete bridging and planar fluorine sites.

Introduction

Luminescent lanthanide-containing materials have practical applications in almost any device involving the artificial production of light: cathode-ray tubes, lamps, and X-ray detectors are well-known examples.[1] Luminescent fluorides are known to exhibit advantageous features compared to their oxide counterparts. These include lower refractive index, wider bandgaps (hence increased transparency range), lower phonon energies (hence lower probability of non-radiative transitions), and longer lifetimes of excited states.[2] Fluorides which can incorporate photoactive lanthanide cations therefore represent an important class of material, and yttrium and lanthanum based fluorides such as YF_3, $LiYF_4$, $NaYF_4$, and LaF_3 have been widely studied for a variety of scientific and technological applications, such as lasers, scintillators, and energy storage phosphors. Other fluoride hosts which may have the potential to incorporate lanthanide cations are also of interest, perhaps the most obvious being those based on the smaller trivalent cations Sc^{3+} and In^{3+}. Compared to the substantial literature on luminescent Y- and La-based fluorides, there is surprisingly little on the corresponding In−F and Sc−F systems. However, elpasolite Rb_2KInF_6 has been shown to incorporate Ce at the In site and displays unusual Ce^{3+}/In^{3+} to Ce^{4+}/In^{+} redox behavior resulting in a reversible change from blue-green to red emission.[3] In the case of scandium fluorides, $LiScF_4$ doped with 1% Er has been shown to display strong far-infrared luminescence, similar to that of the $LiYF_4$ analogue.[4]

The preparation of conventional phosphor powders generally involves high-temperature solid state reactions.[5] However, there has recently been a growing recognition that hybrid organic-inorganic materials, prepared by softer, solvothermal routes offer fruitful new territory in which to search for many functional materials, including luminescent ones.[6] With this in mind, we have begun to explore the use of solvothermal synthetic methods, combined with the exploitation of organic "structure-directing" agents, to prepare a wider range of both yttrium and scandium fluorides.[7−10] Since Sc^{3+} and In^{3+} often display similarities in solvothermal

* To whom correspondence should be addressed. E-mail: pl@st-andrews.ac.uk.
[†] School of Chemistry.
[‡] School of Geography and Geosciences.

(1) Bunzli, J.-C. G.; Piguet, C. *Chem. Soc. Rev.* **2005**, *34*, 1048.
(2) Fouassier C. In *Advanced Inorganic Fluorides*; Nakajima, T, Zemva, B., Tressaud, A., Eds.; Elsevier: Lausanne, 2000.
(3) Chaminade, J. P.; Garcia, A.; Gaewdang, T.; Pouchard, M.; Grannec, J.; Jacquier, B. *Radiat. Eff. Defects Solids* **1995**, *135*, 137.
(4) Tyagi, A. K.; Kohler, J.; Balog, P.; Weber, J. *J. Solid State Chem.* **2005**, *178*, 2620.
(5) Tissue, B. M. *Chem. Mater.* **1998**, *10*, 2837.
(6) Cheetham, A. K.; Rao, C. N. R *Science* **2007**, *318*, 58.
(7) Stephens, N. F.; Slawin, A. M. Z.; Lightfoot, P. *Chem. Commun.* **2004**, 614.
(8) Stephens, N. F.; Lightfoot, P. *Solid State Sci.* **2006**, *8*, 197.
(9) Stephens, N. F.; Lightfoot, P. *J. Solid State Chem.* **2007**, *180*, 260.
(10) Jayasundera, A. C. A.; Finch, A. A.; Townsend, P. D.; Lightfoot, P. *J. Mater. Chem.* **2007**, *17*, 4178.

10.1021/cm802049d CCC: $40.75
Published on Web 10/14/2008

and structural chemistry,[11] we have now expanded our search to organically templated indium fluorides.

The discovery of new luminescent materials containing photo-active lanthanide cations is the key target of this work. As a part of our continuing investigation on new luminescent lanthanide-containing hybrid fluorides, we describe the hydrothermal syntheses, structure determination, ^{19}F and ^{45}Sc MAS NMR studies and photoluminescence properties of the indium fluoride $[C_4H_{14}N_2][InF_5]$ and its scandium analogue $[C_4H_{14}N_2][ScF_5]$ using 1,4-diaminobutane (DAB) as a structure-directing agent.

Experimental Section

Synthesis. $[C_4H_{14}N_2][MF_5]$ (M = In, Sc) and the lanthanide-doped derivatives $[C_4H_{14}N_2][InF_5]$:Ln (Ln = Tb and Eu) were synthesised by solvothermal reaction. The starting materials were indium fluoride (InF_3, 99.99%, Acros Organic), scandium oxide (Sc_2O_3, 99.999%, Stanford Materials), terbium(II) nitrate ($Tb(NO_3)_3$, 99.9%, ProChem), europium oxide (Eu_2O_3, 99.99%, Aldrich), hydrofluoric acid (HF(aq), 48 wt %, Aldrich), ethylene glycol ($OH(CH_2)_2OH$, 99%, Alfa-Aesar), 1,4-diaminobutane (DAB) ($H_2N(CH_2)_4NH_2$, 99.99%, Aldrich), and distilled water. In the case of the lanthanide-doped materials, the samples studied are described in terms of their nominal compositions based on the syntheses; for example, "$[C_4H_{14}N_2][InF_5]$: 5 % Eu" refers to a target composition of $[C_4H_{14}N_2][In_{0.95}Eu_{0.05}F_5]$. In fact, the actual product compositions generally show significantly lower lanthanide contents, as described later. For $[C_4H_{14}N_2][InF_5]$ **1**, InF_3 (0.1717 g, 1 mmol) was placed into a polypropylene bottle with 1.0 mL (50 mmol) of HF(aq) and 5 mL (280 mmol) of H_2O. This was heated at 100 °C for 2 h, and then the contents of the bottle were transferred to a Teflon lined stainless steel autoclave, with the addition of 3 mL of ethylene glycol, 3 mL of H_2O, and 2.0 mL (20 mmol) of DAB, to give a pH of 4. The autoclave was heated at 190 °C for 48 h. The product was filtered, washed with water, and dried at room temperature to give colorless plate-like crystals. Elemental analysis, obsd (calcd): C, 14.51 (16.02); H, 4.81 (4.70); N, 9.41 (9.34)%. For $[C_4H_{14}N_2][ScF_5]$ **2**, Sc_2O_3 (0.1379 g, 1 mmol) was placed in a polypropylene bottle with 2.0 mL (100 mmol) of HF and 5 mL (280 mmol) of H_2O. This was heated at 100 °C for 2 h, and then the contents were transferred into a Teflon lined stainless steel autoclave, with addition of 5 mL (100 mmol) ethylene glycol and 2.0 mL (20 mmol) of DAB to give a pH of 6. The autoclave was heated at 190 °C for three days. The product was filtered, washed with water, and dried at room temperature to give colorless crystals. Elemental analysis for $[C_4H_{14}N_2][ScF_5]$, obsd (calcd): C, 20.87 (20.88); H, 5.99 (6.13); N, 12.03 (12.17)%. Lanthanide doped materials were prepared in an analogous manner.

Initial Characterization. Crystallinity and phase purity were determined by powder X-ray diffraction (XRD) using a Stoe STADI/P transmission diffractometer using Cu $K\alpha_1$ radiation, with a 2θ range of 5 to 100° and a data collection time of 15 h (see Supporting Information). SEM/EDX studies (Jeol JSM 5600) were carried out for qualitative and quantitative (based on 20 independent analyses of each samples) measurements for doped lanthanides (Eu and Tb) in the $[C_4H_{14}N_2][InF_5]$ host (Figure 1).

Crystal Structure Determination. Single-crystal X-ray diffraction data were collected using synchrotron radiation on beamline 11.3.1 at the Advanced Light Source, Berkeley, U.S.A., for compound **1** and Rigaku Mercury CCD equipped with graphite monochromated Mo Kα radiation for **2**. An absorption correction was applied in both cases. The structures were solved by direct methods and refined by standard techniques, using the SHELX-97 and WinGX packages. All non-hydrogen atoms were refined with anisotropic thermal parameters. Hydrogen atoms attached to C and N were located at geometrically calculated positions and refined with isotropic thermal parameters. Other crystal data and experimental parameters are summarized in Tables 1 and 2.

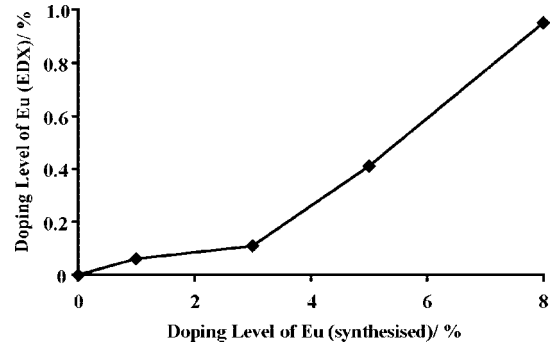

Figure 1. Calibration of nominal dopant levels based on the synthesis, to EDX-determined Eu content for Eu^{3+}-doped **1**.

Table 1. Crystallographic Data for $[C_4H_{14}N_2][InF_5]$ 1 and $[C_4H_{14}N_2][ScF_5]$ 2

formula	$[C_4H_{14}N_2][InF_5]$	$[C_4H_{14}N_2][ScF_5]$
F_w	299.99	230.12
space group	*Ibam*	*Ibam*
a [Å]	9.324 (2)	9.353(3)
b [Å]	11.391(2)	11.433 (1)
c [Å]	8.401(2)	8.226(4)
V [Å^3]	892.2(3)	879.7(5)
Z	4	4
ρ_{calcd} [g cm^{-3}]	1.890	1.738
μ [mm^{-1}]	2.660	0.869
crystal size [mm]	not measured	0.1 × 0.15 × 0.2
F(000)	584	472
reflns collected	4369	2280
independent reflns	708	451
R_{int}	0.0499	0.0313
obsd data [$I > 2\sigma(I)$]	630	421
data/restraints/parameters	708/0/35	451/0/35
GOF on F^2	0.965	1.906
R1, *wR*2 ($I > 2\sigma(I)$)	0.0254, 0.0679	0.0415, 0.1173
R1, *wR*2 (all data)	0.0271, 0.0710	0.0571, 0.1656

Table 2. Selected Bond Lengths (Å) for 1 and 2

bond	bond Length, Å
In—F(1) × 4	2.0486(18)
Sc—F(1) × 4	2.008(2)
In—F(2) × 2	2.1002(4)
Sc—F(2) × 2	2.0566(10)

Thermal Analysis. Themogravimetric analysis was carried out on a TA Instruments SDT2960 dual TGA/DTA, in the temperature range 30−750 °C, under flowing N_2 at a heating rate of 5 °C min^{-1}. The TGA/DTA of **2** (Supporting Information) shows that a single step weight loss occurs from 263 °C to 387 °C, which corresponds to a loss of the organic template (DAB) and HF:

$$[C_4H_{14}N_2][ScF_5] \rightarrow ScF_3 + C_4H_{12}N_2 + 2HF$$

Residual ScF_3 (PDF no. 44-1096) was confirmed by powder XRD.

Solid State NMR. The ^{45}Sc and ^{19}F spectra were recorded on a Varian Infinity Plus 500 MHz spectrometer using a Chemagnetics

(11) Miller, S. R.; Slawin, A. M. Z.; Wormald, P.; Wright, P. A. *J. Solid State Chem.* **2005**, *178*, 1738.

3.2 mm HFXY probe with Larmor frequency of 121.450 MHz and 470.385 MHz, respectively. The ^{45}Sc chemical shifts are reported with respect to an external $ScCl_3$ solution sample at ($\delta_{Sc} = 0$)[12] and magic angle spinning at 12 kHz. The ^{19}F spectral reference was C_6F_6 ($\delta_F = -166.4$ ppm with respect to $CFCl_3$). Spectra were recorded at a magic angle spinning of 23 kHz. The excitation pulse was selected as 1 μs, and the Hahn echo sequence was used for ^{45}Sc and a direct polarization pulse of 4 μs for ^{19}F acquisition. For ^{45}Sc spectra both ^{1}H and ^{19}F decoupling was applied, and for the ^{19}F spectra, ^{1}H decoupling. Analytical simulations were performed using DMFIT.[13]

Luminescence Measurements. Luminescence data were collected at room temperature on a SPEX Fluorolog 2 photoluminescence spectrometer. The primary excitation is from a 450 W xenon lamp, the radiation from which is passed through a 0.22 m SPEX 1680 monochromator to achieve a monochromatic tunable spot. The luminescence from the sample is passed through a 0.22 m SPEX 1681 double monochromator, and light intensity is measured using a red-sensitive Hamamatsu R928 photomultiplier tube (PMT). Reflections of the primary radiation are removed by a series of long-pass filters. The PMT is cooled by a Peltier device, and the emission spectrometer has a wavelength resolution of ~0.5 nm using the slit widths of the present study. The system is controlled using software written in LabVIEW at the University of St. Andrews. Excitation and emission spectra were corrected for system response. Lifetime measurements were made on the same system using UV excitation from a bank of 8 Farnell 395nm UV LEDs, the radiation from which is passed through a Comar 380 nm interference filter to remove a small amount of visible radiation. The LEDs are powered by a benchtop supply controlled by a Thurlby Thandar TGP 110 pulse generator to give pulsed primary UV radiation. The luminescence from the sample is passed through the emission monochromator, and the signal from the PMT is measured in the time domain using a Becker-Hickl PMS-400A gated photon counting card controlled by software provided by the manufacturers. The counting card has a minimum bin time of 250 ns, but analysis of the radiation directly from the LED shows it has a 1 μs decay time when switched with a square wave function. Hence resolution of luminescence decays with lifetimes <10 μs is not attempted on this instrument.

Results and Discussion

Structural Description. The crystal structure of $[C_4H_{14}N_2][MF_5]$ (M = In, Sc) is composed of infinite trans vertex sharing anionic $(MF_5)_\infty$ chains running parallel to the *c* axis, which are separated by H-bonded $[C_4H_{14}N_2]^{2+}$ moieties (N(1)−H(3)···F1 = 2.678 Å). The building unit (Figure 2) includes one distinct octahedral M crystallographic site with 222 point symmetry and two distinct F sites ("terminal" and "bridging" relative to the chain direction). The bridging M−F bond lengths are somewhat longer than the terminal ones as is normally found in such structural moieties (Table 2). Figure 3 shows the unit cell packing and arrangements of the inorganic chains and organic moieties. The trans-vertex sharing $(MF_5)_\infty$ chain is a relatively common structural element in fluoride chemistry, occurring, for example, in inorganic types such as $A^{II}M^{III}F_5$ and $A^{I}_2MF_5$[14] and also in organically templated types such as $[enH_2][ScF_5]$.[8]

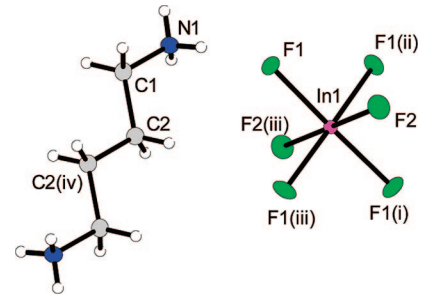

Figure 2. Building unit of the crystal structure of **1**. Symmetry operators: (i) $1 - x, -y, -z$; (ii) $1 - x, y, 1/2 - z$; (iii) $x, -y, 1/2 - z$; and (iv) $-x, -y, -z$.

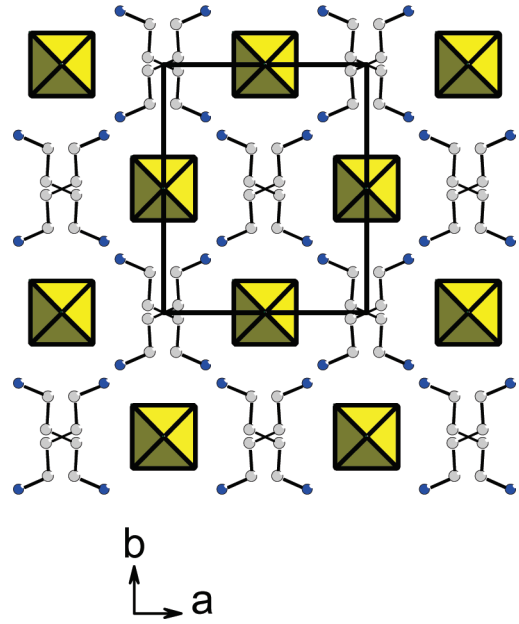

Figure 3. Crystal packing of **1,** viewed down the$[InF_5]$ chain axis. Hydrogen atoms of the $[C_4H_{14}N_2]$ moiety not shown.

Solid State NMR. Scandium has several advantageous NMR properties, a single naturally occurring isotope ^{45}Sc ($I = 7/2$) with 100% abundance and a favorable gyromagnetic ratio of 6.5088×10^7 rad^{-1} T^{-1} S^{-1}. The ^{45}Sc quadrupole moment (Q) is also relatively small, 0.22×10^{-28} m^2, although ^{45}Sc spectra can often exhibit powder patterns resulting from the anisotropic interactions.[15]

Kim et al.[12] have shown that the chemical shift and quadrupolar coupling constant in scandium oxides are sensitive to the local structure, the isotropic chemical shift being dictated largely by a near-neighbor coordination environment, with a difference of 150 ppm being seen between six- and eight-coordinated scandium. Little is known about the corresponding structural influences in scandium fluorides, although the isotropic chemical shift, δ_{iso}, for regular octahedral Sc in ScF_3 is reported at −52 ppm and the quadrupolar coupling constant, C_Q, as 1.3 MHz.[16] Furthermore, the sensitivity and abundance of the fluoride in these compounds should also provide the opportunity to acquire information on the scandium coordination and differentiate between terminal and bridging anions, which

(12) Kim, N.; Hsieh, C.-H.; Stebbins, J. F. *Chem. Mater.* **2006**, *18*, 3855.
(13) Massiot, D.; Fayon, F.; Capron, M.; King, I.; Le Calvé, S.; Alonso, B.; Durand, J.-O.; Bujoli, B.; Gan, Z.; Hoatson, G. *Magn. Reson. Chem.* **2002**, *40*, 70.
(14) Massa, W.; Babel, D. *Chem. Rev.* **1988**, *88*, 275.
(15) Rossini, A. J.; Schurko, R. W. *J. Am. Chem. Soc.* **2006**, *128*, 10391.
(16) Lo, A. Y. H.; Sudarsan, V.; Sivakumar, S.; van Veggel, F.; Schurko, R. W. *J. Am. Chem. Soc.* **2007**, *129*, 4687.

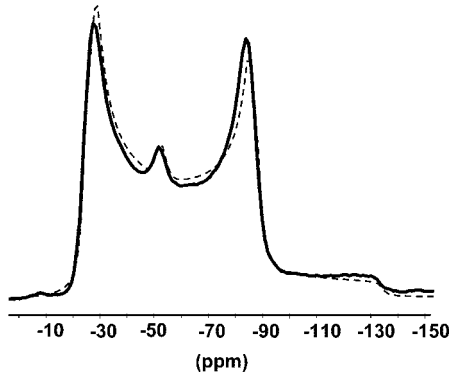

Figure 4. Experimental (full line) and fitted (dashed line) ^{45}Sc SSNMR spectrum of $[C_4H_{14}N_2][ScF_5]$ with ^{19}F decoupling.

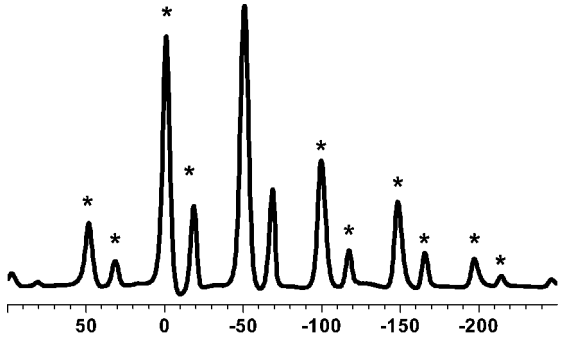

Figure 5. ^{19}F 23 kHz MASNMR spectrum of $[C_4H_{14}N_2][ScF_5]$. Signals with asterisks are spinning sidebands, and integration of these signals and sidebands gives a ratio of 4:1 for signals at −52.3 and −69.9 ppm, respectively.

is often very difficult to obtain from related scandium oxide compounds.

Figure 4 shows the ^{45}Sc of **2** with a typical line-shape dominated by quadrupolar interaction. Analysis using DMFIT gives values $C_Q = 9.01$ MHz, $\eta = 0.06$, and $\delta_{iso} = -8.09$ ppm indicating only one ^{45}Sc species in the sample, in agreement with the X-ray data. The signal near −50 ppm is consistent with a trace amount of ScF_3 impurity, although this is not observable by powder XRD.

The ^{19}F spectrum (Figure 5) shows two signals, one assigned to the terminal fluorine F(1) at −52.3 ppm and $\upsilon_{1/2} = 2.7$ kHz and one at −69.9 ppm with $\upsilon_{1/2} = 1.8$ kHz to the bridging fluorine, F(2). The integral values, including the spinning sideband intensities, are in a ratio 4:1, consistent with the crystal structure. The relative chemical shifts follow the same trend as those for bridging versus terminal F atoms in, for example, the aluminium fluoride chain structure $CaAlF_5$.[17] One might expect the presence of ^{19}F−^{45}Sc coupling in the ^{19}F spectra, but this is not often observed due to the line width, which is often broadened due to fast quadrupolar relaxation.

Photoluminescence. The photoluminescence of doped samples of **1** with nominal compositions $[C_4H_{14}N_2][InF_5]$: 5% Eu^{3+} and $[C_4H_{14}N_2][InF_5]$: 8% Tb^{3+} in the visible region were investigated at room temperature. At compositions up to 20% Eu^{3+} or 15% Tb^{3+}, there is no evidence of any impurity phase detectable by powder XRD; InF_3 appears as a detectable impurity at dopant levels higher than these, occasionally with a trace amount of another, unidentified phase (Supporting Information). EDX confirms that the InF_3 phase does *not* accommodate significant amounts of lanthanide dopant. The EDX analyses of the X-ray pure doped phase **1** samples reveal average lanthanide concentrations significantly lower than the ideal ones and also a large inhomogeneity within each sample. For the 5% Eu^{3+} sample the EDX analysis gives an average 0.9% Eu, and for the 8% Tb^{3+} sample the analysis reveals only 0.7% Tb.

Eu^{3+} and Tb^{3+} absorb ultraviolet radiation efficiently through a series of electronic transitions that promote electrons to $^5D_0$ and $^5D_4$ excited states, respectively, and these are deactivated to the multiplet ^7F_J states radiatively via emission of visible radiation. In general, electric dipole f−f transitions in free $4f^n$ ions are parity forbidden but become partially allowed by mixing with orbitals having different parities because of an odd crystal field component. The excitation spectrum of $[C_4H_{14}N_2][InF_5]$: 5% Eu^{3+} recorded at room temperature (Figure 6) displays a series of sharp lines assigned to the $^7F_{0,1} \rightarrow {}^5H_6$, $^5D_4$, $^5G_2$, $^5L_6$, $^5D_3$, and $^5D_2$ Eu^{3+} intra-4f transitions.[18] $[C_4H_{14}N_2][InF_5]$:Eu^{3+}exhibits an intense, characteristic emission spectrum of Eu^{3+} ions upon excitation with a radiation of 395 nm. As shown in Figure 6, transitions from the excited $^5D_0$ state to the different J levels of the lower ^7F state were observed in the emission spectrum ($J = 0-4$), that is, $^5D_0 \rightarrow {}^7F_0$ at 578 nm, $^5D_0 \rightarrow {}^7F_1$ at 592.5 nm, $^5D_0 \rightarrow {}^7F_2$ at 614 nm, $^5D_0 \rightarrow {}^7F_3$ at 650.5 nm, and $^5D_0 \rightarrow {}^7F_4$ at 698.5 nm. Many transitions are in detail a series of lines. The $^5D_0 \rightarrow {}^7F_0$ (578 nm) transition cannot be split by the crystal field, and its profile gives information on the number of different coordination sites accommodating the Eu^{3+} ion. The presence of a single $^5D_0 \rightarrow {}^7F_0$ band, characterized by a Lorentzian shape in the high-resolution luminescence spectrum of the $[C_4H_{14}N_2][InF_5]$: Eu^{3+}, indicates that the Eu^{3+} ion occupies a single site.[18] The $^5D_0 \rightarrow {}^7F_1$ transition of Eu^{3+} is of magnetic-dipole nature and insensitive to site symmetry, while $^5D_0 \rightarrow {}^7F_2$ is of electric-dipole nature and very sensitive to site symmetry. The emission intensity of the $^5D_0 \rightarrow {}^7F_1$ transition is much stronger than that of the $^5D_0 \rightarrow {}^7F_2$ transition, consistent with Eu^{3+} ions at a high-symmetry site, in agreement with the crystal structure analysis. The In site has D_2 (222) point symmetry, although the actual geometry is also very close to centrosymmetric. For a single Eu^{3+} at a 222 point symmetry site, we also expect the $^5D_0 \rightarrow {}^7F_J$ energy bands to be split into $2J + 1$ sublevels (Stark sublevels). Observation of the detail within the luminescence shows three subpeaks at the 585 nm emission ($J = 1$) and five for that at 614 nm ($J = 2$). These observations are consistent with Eu^{3+} predominantly being accommodated at the In site.

$[C_4H_{14}N_2][InF_5]$: 8% Tb^{3+} exhibits a Tb^{3+} emission spectrum containing the expected sequence of $^5D_4 \rightarrow {}^7F_J$ ($J = 2-6$) transitions upon excitation at, for example, 272 nm (Figure 7). The spectrum is dominated by the green $^5D_4 \rightarrow {}^7F_5$ transition at 543.5 nm. The other bands at ∼489, 587,

(17) Body, M.; Silly, G.; Legein, C.; Buzare, J. Y.; Calvayrac, F.; Blaha, P. *J. Solid State Chem.* **2005**, *178*, 3655.

(18) Gaft, M.; Reisfeld, R.; Panczer, G. *Luminescence Spectroscopy of Minerals and Materials*; Springer: Berlin, 2005.

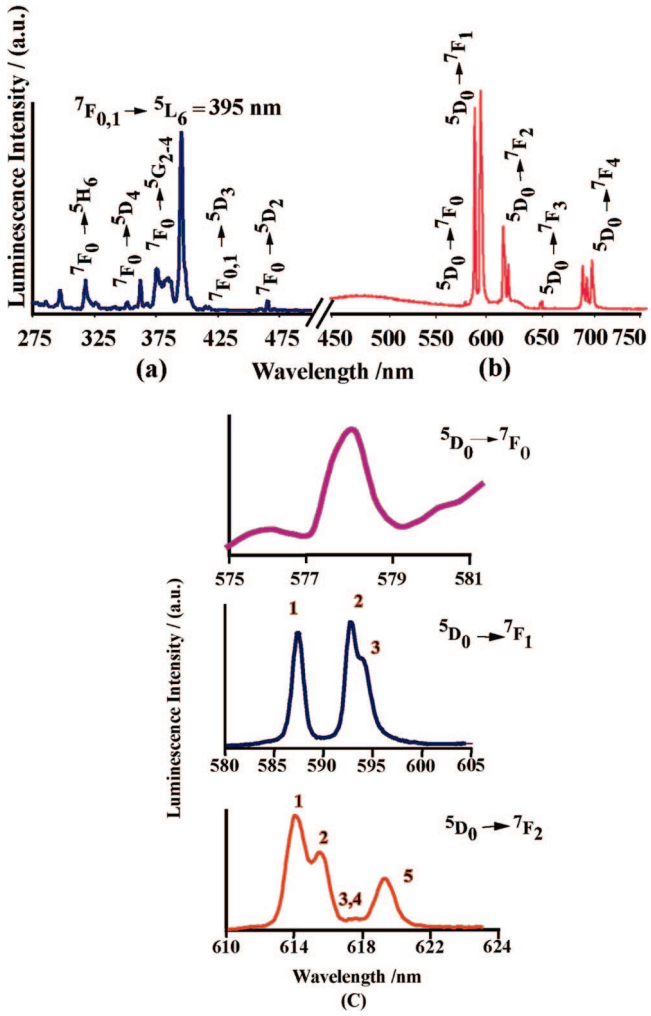

Figure 6. Photoluminescence spectra of $[C_4H_{14}N_2][InF_5]$: 5% Eu^{3+} at 298 K: (a) excitation spectrum with emission in the $^5D_0 \rightarrow {}^7F_1$ transition of the Eu^{3+} ion at 592.5 nm, (b) emission spectrum monitored at 395 nm, and (c) Stark splittings of the $^5D_0 \rightarrow {}^7F_n$ transitions, showing the expected $(2J + 1)$ lines for 222 site symmetry.

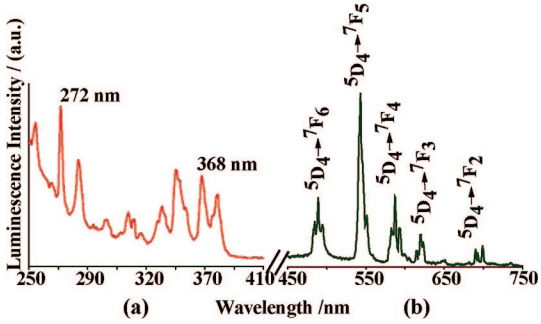

Figure 7. Photoluminescence spectra of $[C_4H_{14}N_2][InF_5]$: 8% Tb^{3+} at 298 K: (a) excitation spectrum with emission in the $^5D_4 \rightarrow {}^7F_5$ transition of the Tb^{3+} ion at 543.5 nm and (b) emission spectrum monitored at 272 nm.

619.5, and 690 nm correspond to transitions from the $^5D_4$ state to $^7F_6$, $^7F_4$, $^7F_3$, and $^7F_2$ levels, respectively.[18]

Figure 8 shows the effect of Eu^{3+} dopant level on the normalized luminescence intensity of the most dominant emission peak, 592.5 nm, with respect to the prominent excitation wavelength 395 nm. A maximum luminescence at ~5% nominal Eu^{3+} doping in $[C_4H_{14}N_2][InF_5]$ is observed. An analogous study of nominal doping level vs normalized luminescent intensity of Tb^{3+}-doped$[C_4H_{14}N_2][InF_5]$ shows

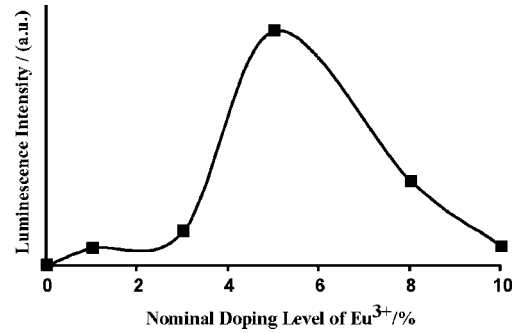

Figure 8. Luminescence intensity versus nominal Eu^{3+} content for $[C_4H_{14}N_2][InF_5]$: Eu^{3+}.

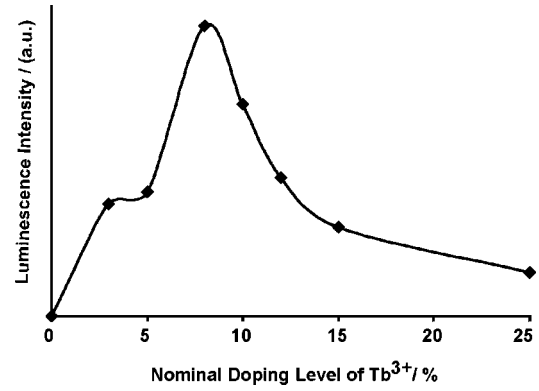

Figure 9. Luminescence intensity versus nominal Tb^{3+} content for $[C_4H_{14}N_2][InF_5]$: Tb^{3+}.

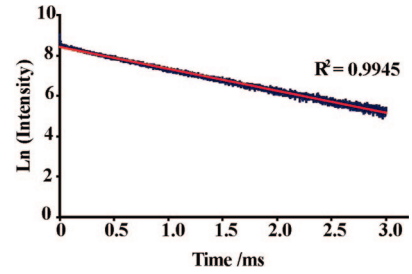

Figure 10. Luminescence decay curve for $[C_4H_{14}N_2][InF_5]$: 5% Eu^{3+}.

similar features (Figure 9), with ~8% Tb^{3+} providing the optimal dopant level for the $[C_4H_{14}N_2][InF_5]$ host structure.

The luminescence decay curves of $[C_4H_{14}N_2][InF_5]$: 5% Eu^{3+} were obtained at room temperature. The decay curves (Figure 10) are well fitted into a single-exponential function as $I = I_0 \exp(-t/\tau)$, consistent with one average local environment of Ln^{3+} sites in the structure. The corresponding lifetime for $[C_4H_{14}N_2][InF_5]$: 5% Eu^{3+} is about 1.24 ms. $[C_4H_{14}N_2][InF_5]$: 5% Eu^{3+} has a relatively long luminescence lifetime which is comparable to other corresponding Eu^{3+} complexes, indicating that non-radiative transitions are not dominating the decay properties.

Co-doping provides important insights into the transfer of energy between different lanthanides and the coupling of the lattice to the lanthanide ions. When Tb:Eu is 1:1 ($[C_4H_{14}N_2][InF_5]$: 1% Eu^{3+}, 1% Tb^{3+}), both absorption and emission are dominated by Eu^{3+} (Figure 11b). However the photoluminescence intensity of the Eu^{3+} emission, as measured by the $^5D_0 \rightarrow {}^5F_1$ transition, is more than double the intensity of the singly doped material ($[C_4H_{14}N_2][InF_5]$: 1% Eu^{3+}) with

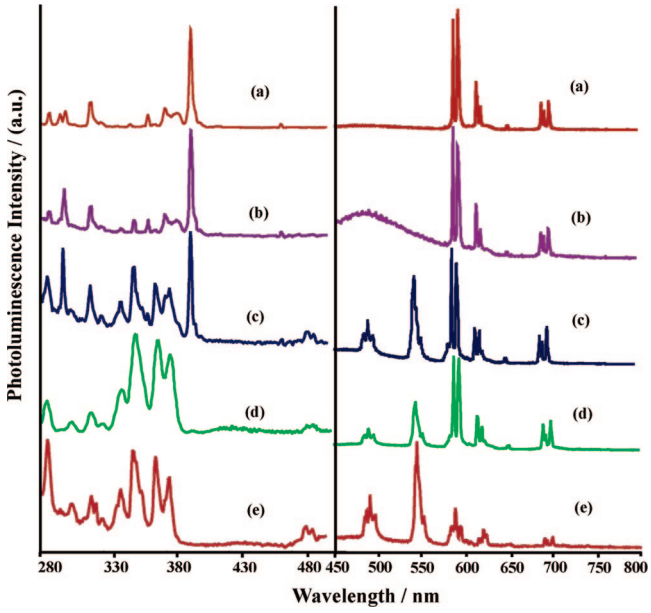

Figure 11. Excitation (left) and emission (right) spectra for co-doped $[C_4H_{14}N_2][InF_5]$: Eu^{3+}, Tb^{3+} at various Eu^{3+}/Tb^{3+} ratios: (a) 5% Eu^{3+}, 0% Tb^{3+}; (b) 1% Eu^{3+}, 1% Tb^{3+}; (c) 1% Eu^{3+}, 15% Tb^{3+}; (d) 1% Eu^{3+}, 20% Tb^{3+}; and (e) 0% Eu^{3+}, 8% Tb^{3+}.

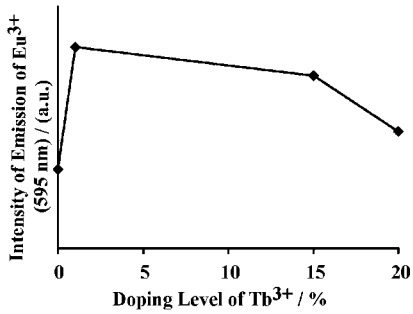

Figure 12. Enhancement of Eu^{3+} luminescence by co-doping of Tb^{3+}.

the same Eu^{3+} content (Figure 12). Hence, the Tb^{3+} ion is enhancing the efficiency of the luminescence due to Eu^{3+}. We infer that the energy involved in the luminescence of the co-doped samples is absorbed on Eu^{3+} but transferred to Tb^{3+} and then returned to Eu^{3+}. Such energy transfers may be directly from Tb^{3+} to Eu^{3+} or, perhaps more likely, involve transfer of the electron via the host lattice. By the same token, it may be that the lattice is involved in energy transfers within singly doped materials and that the most efficient absorption and recombination on the same ion is not an intra-ion process. To understand further the influence of Tb^{3+} content on both the absorption and the emission behavior, samples of nominal composition $[C_4H_{14}N_2][InF_5]$: 1% Eu^{3+}, 15% Tb^{3+} (Figure 11c) and $[C_4H_{14}N_2][InF_5]$: 1% Eu^{3+}, 20% Tb^{3+} (Figure 11d) were also studied. The photoluminescence character of $[C_4H_{14}N_2][InF_5]$: 1% Eu^{3+}, 15% Tb^{3+} (EDX value = 0.3% Eu and 6.1% Tb) shows a combination of Tb^{3+} and Eu^{3+} absorption and a combination of Tb^{3+} and Eu^{3+} emission. On the other hand, $[C_4H_{14}N_2][InF_5]$: 1% Eu^{3+}, 20% Tb^{3+} (EDX value = 0.7% Eu and 9.5% Tb) is dominated by Tb^{3+} absorption, with Eu^{3+} absorption being almost unobservable. This, however, still gives rise to a strong combination of both Tb^{3+} and Eu^{3+} emission. The emission line at 543 nm is characteristic of $^5D_4 \rightarrow {}^7F_5$ transition of Tb^{3+} ion, and emission lines at 595 nm, 587 nm, and 614 nm are characteristic emissions for Eu^{3+} with respect to transition from $^5D_0 \rightarrow {}^7F_J$ ($J = 2$, 1, and 3). It is clear that Tb^{3+} acts as a sensitizer for Eu^{3+} emission under this co-doping regime.

Conclusions

The new hybrid fluoride chain compound$[C_4H_{14}N_2][InF_5]$ **1** and its Sc analogue **2** have been synthesised. Eu^{3+} and Tb^{3+} doping of **1** reveals an optimal photoluminescence intensity for a nominal 5% Eu^{3+} concentration and 8% Tb^{3+} concentration, although the experimentally determined compositions show significantly smaller lanthanide contents. For Eu^{3+} - doped material, the absence of a doublet in the $^5D_0 \rightarrow {}^7F_0$ transition and the lifetime measurements are both consistent with one Ln^{3+} site, and the ratio of the integrated intensities of the $^5D_0 \rightarrow {}^7F_2$ and $^5D_0 \rightarrow {}^7F_1$ transitions is consistent with that site having the same point symmetry as In^{3+} and Sc^{3+} in the parent crystal structures. By studying co-doped crystals of varying Eu^{3+} / Tb^{3+} content it is found that Tb^{3+} enhances the luminescence of Eu^{3+} in this host; i.e. the Tb^{3+} ion acts as an efficient sensitiser to the Eu^{3+} activator in the co-doped materials.

Acknowledgment. We thank Prof. Alex Slawin, Dr. Yang Li, and Dr. David Wragg for collection of the single crystal X-ray data and the University of St. Andrews and EPSRC for funding.

Supporting Information Available: Crystallographic information (CIF), thermogravimetric analysis, and powder X-ray diffraction data (PDF). This material is available free of charge via the Internet at http: //pubs.acs.org.

CM802049D